Spin Transfer Torques in MnSi at Ultralow Current Densities

F. Jonietz, *et al.*

Science **330**, 1648 (2010);
DOI: 10.1126/science.1195709

fully spin-down for V_g about the degeneracy point (A) and fully spin-up for V_g about the degeneracy point (B) in Fig. 1E. Accordingly, we calculate β from the conductance peaks along the two dotted lines in Fig. 2D, obtaining β ~ 0.26, which is close to P_F ~ 0.28 and indicates a filtering efficiency larger than 0.9.

Lastly, we stress that the spin-ratchet effect is related to quasi-particle tunneling through the high-transparency junction (*22*). To further show this, we fabricated normal super conductor ferromagnet (NSF) devices with the normal metal lead made of Cu connected to the low-transparency junction. Here, $R_l \approx 650$ kΩ and $R_r \approx 70$ kΩ. Because the high-transparency tunnel barrier connected to the ferromagnetic lead controls the transport, β should remain close to P_F, when calculated as in Fig. 3D. Moreover, because R_r in this device is estimated to be of the same order of magnitude as that of the FSF device, the conductance peaks should not be substantially affected. Both these observations agree with the experimental *dI*/*dV* results shown in Fig. 4. At $B = 0$ (Fig. 4A), β is again zero within the sensitivity of our measurements and, at $B > B_{SR}$ (Fig. 4B), β ~ 0.25 ~ P_F, whereas the magnitudes of the conductance peaks compare well with those shown in Fig. 3.

Spin ratchets represent a fundamentally new approach for spin current generation and detection; thus, our research paves the way for a new means to study spin-related phenomena. Because the spin ratchets presented here work at the single-electron level, they can, for example, be used to initialize and read out the state of spin-based quantum bits (*8*) or to identify the spin orientation of single electrons in a test of the Einstein-Podolsky-Rosen paradox (*24*) with spin-entangled electrons (*25*–*29*).

References and Notes

1. P. Hänggi, F. Marchesoni, F. Nori, *Ann. Phys.* **14**, 51 (2005).
2. P. Reimann, *Phys. Rep.* **361**, 57 (2002).
3. P. Hänggi, F. Marchesoni, *Rev. Mod. Phys.* **81**, 387 (2009).
4. A. M. Song *et al.*, *Phys. Rev. Lett.* **80**, 3831 (1998).
5. H. Linke *et al.*, *Science* **286**, 2314 (1999).
6. J. E. Villegas *et al.*, *Science* **302**, 1188 (2003).
7. I. Žutić, J. Fabian, S. Das Sarma, *Rev. Mod. Phys.* **76**, 323 (2004).
8. D. D. Awschalom, D. Loss, N. Samarth, *Semiconductor Spintronics and Quantum Computation* (Springer-Verlag, Berlin, 2002).
9. M. Scheid, D. Bercioux, K. Richter, *N. J. Phys.* **9**, 401 (2007).
10. S. Smirnov, D. Bercioux, M. Grifoni, K. Richter, *Phys. Rev. Lett.* **100**, 230601 (2008).
11. M. E. Flatté, *Nat. Phys.* **4**, 587 (2008).
12. M. Scheid, A. Lassl, K. Richter, *EPL* **87**, 17001 (2009).
13. D. V. Averin, Y. V. Nazarov, *Phys. Rev. Lett.* **69**, 1993 (1992).
14. M. T. Tuominen, J. M. Hergenrother, T. S. Tighe, M. Tinkham, *Phys. Rev. Lett.* **69**, 1997 (1992).
15. T. M. Eiles, J. M. Martinis, M. H. Devoret, *Phys. Rev. Lett.* **70**, 1862 (1993).
16. F. W. J. Hekking, L. I. Glazman, K. A. Matveev, R. I. Shekhter, *Phys. Rev. Lett.* **70**, 4138 (1993).
17. G. Schön, in *Quantum Transport and Dissipation*, T. Dittrich *et al.*, Eds. (Wiley, Weinheim, Germany, 1998), chap. 3.
18. A. J. Ferguson, S. E. Andresen, R. Brenner, R. G. Clark, *Phys. Rev. Lett.* **97**, 086602 (2006).
19. Materials and methods are available as supporting material on *Science* Online.
20. S. O. Valenzuela, M. Tinkham, *Nature* **442**, 176 (2006).
21. S. O. Valenzuela, *Int. J. Mod. Phys. B* **23**, 2413 (2009).
22. A zero *dI*/*dV* below the quasi-particle thresholds suggests that the Andreev cycle (Fig. 1C) and cotunneling processes (*13*) are suppressed. Integration of *dI*/*dV* results in a current plateau I_p ~ 5.8 pA beyond the thresholds. Because the current is limited by Γ_r^{oe}, $I_p \approx e\Gamma_r^{oe}$ ~ 5 pA, which is in reasonable agreement with the measured value. This indicates that transport is dominated by tunneling events in the r junction.
23. The decrease in V_0 with increasing B is larger than expected if only E_Z is considered; in which case, the ratchet effect should occur at $B_{SR} \approx 2.3$ T. This is due to a reduction of Δ by residual orbital depairing. When such a reduction is considered, Δ(1 T) = 272 μeV, V_0(1 T) = $2[\Delta(1\text{ T}) - E_c]/e - E_Z/e \approx 88$ μV is close to the measured value. Moreover, considering Δ(1.5 T) = 256 μeV, we estimate $B_{SR} = [\Delta(1.5\text{ T}) - E_c]/(g\mu_B) \approx 1.48$ T, in agreement with the observed result.
24. A. Einstein, B. Podolsky, N. Rosen, *Phys. Rev.* **47**, 777 (1935).
25. C. Bena, S. Vishveshwara, L. Balents, M. P. A. Fisher, *Phys. Rev. Lett.* **89**, 037901 (2002).
26. D. S. Saraga, D. Loss, *Phys. Rev. Lett.* **90**, 166803 (2003).
27. L. Hofstetter, S. Csonka, J. Nygård, C. Schönenberger, *Nature* **461**, 960 (2009).
28. P. Cadden-Zimansky, J. Wei, V. Chandrasekhar, *Nat. Phys.* **5**, 393 (2009).
29. L. G. Herrmann *et al.*, *Phys. Rev. Lett.* **104**, 026801 (2010).

30. We gratefully acknowledge discussions with and support from M. Tinkham and thank I. Žutić and Y. Tserkovnyak for discussions and W. D. Oliver, P. Gambardella, and A. Bachtold for a critical reading of the manuscript. This research was supported in part by the Spanish Ministerio de Ciencia e Innovación (MAT2010-18065, FIS2009-06671-E). Samples were made at the Center for Nanoscale Systems, Harvard University.

Supporting Online Material

www.sciencemag.org/cgi/content/full/330/6011/1645/DC1
Materials and Methods
SOM Text
Figs. S1 to S3
References

9 August 2010; accepted 9 November 2010
10.1126/science.1196228

Spin Transfer Torques in MnSi at Ultralow Current Densities

F. Jonietz,[1] S. Mühlbauer,[1,2] C. Pfleiderer,[1]* A. Neubauer,[1] W. Münzer,[1] A. Bauer,[1] T. Adams,[1] R. Georgii,[1,2] P. Böni,[1] R. A. Duine,[3] K. Everschor,[4] M. Garst,[4] A. Rosch[4]

Spin manipulation using electric currents is one of the most promising directions in the field of spintronics. We used neutron scattering to observe the influence of an electric current on the magnetic structure in a bulk material. In the skyrmion lattice of manganese silicon, where the spins form a lattice of magnetic vortices similar to the vortex lattice in type II superconductors, we observe the rotation of the diffraction pattern in response to currents that are over five orders of magnitude smaller than those typically applied in experimental studies on current-driven magnetization dynamics in nanostructures. We attribute our observations to an extremely efficient coupling of inhomogeneous spin currents to topologically stable knots in spin structures.

The discovery of the effect of giant magnetoresistance, now used commercially in the hard disk drive industry, is widely recognized as the starting point of the field of spintronics. It represents the first example of electric currents controlled efficiently by spin structures. The complementary process of so-called spin transfer torques, where magnetic structures and textures are manipulated by electric currents (*1*, *2*), appears to be even more promising. For instance, strong current pulses allow the movement of ferromagnetic domain walls (*3*, *4*), the switching of magnetic domains in multilayer devices (*5*, *6*), the induction of microwave oscillations in nanomagnets (*7*), and the switching of ferromagnetic semiconductor structures (*8*). However, the typical current densities required to create observable spin transfer torques in present-day studies exceed 10^{11} A m^{-2}. Because this implies extreme ohmic heating, it was generally believed that spin torque effects can be studied exclusively in nanostructures. We report the observation of spin transfer torques in a bulk material, the skyrmion lattice phase of MnSi. The spin transfer torques appear when the current density exceeds an ultralow threshold of ~10^6 A m^{-2}, five orders of magnitude smaller than those used typically in experimental studies on current-driven magnetization dynamics in ferromagnetic metals and semiconductors.

The skyrmion lattice in chiral magnets, like MnSi and related B20 compounds, was only recently discovered in neutron-scattering studies (*9*–*12*) and confirmed to exist in Lorentz force microscopy for $Fe_{1-x}Co_xSi$ (x = 0.5) (*13*). It represents a new form of magnetic order that may be viewed as a crystallization of topologically stable knots of the spin structure that shares remarkable similarities with the mixed state in type II superconductors. For zero magnetic field (Fig. 1A), helimagnetic order appears in MnSi below the critical temperature T_c = 29.5 K.

[1]Physik-Department E21, Technische Universität München, D-85748 Garching, Germany. [2]Forschungsneutronenquelle Heinz Maier-Leibnitz (FRM II), Technische Universität München, D-85748 Garching, Germany. [3]Institute for Theoretical Physics, Utrecht University, 3584 CE Utrecht, Netherlands. [4]Institute of Theoretical Physics, University of Cologne, D-50937 Cologne, Germany.

*To whom correspondence should be addressed. E-mail: christian.pfleiderer@frm2.tum.de

In a small magnetic field, the skyrmion lattice stabilizes in a pocket below T_c, also known as the A phase. The spin structure of the skyrmion lattice in MnSi consists of a hexagonal lattice of magnetic vortex lines oriented parallel to the magnetic field **B** (Fig. 1A, inset).

Skyrmion lattices in chiral magnets are attractive for studies of spin torque effects, because they are coupled very weakly to the atomic crystal structure (*9*) and may be expected to pin very weakly to disorder. In addition, electric currents couple very efficiently to skyrmions as follows. When the conduction electrons in a metal move across a magnetic texture, their spin follows the local magnetization adiabatically. Spins that change their orientation pick up a quantum mechanical phase, the Berry phase, that may be viewed as an Aharonov-Bohm phase arising from a fictitious effective field (*14*–*16*) $\mathbf{B}^i_{\mathrm{eff}} = \frac{\Phi_0}{8\pi} D_{ijk}\hat{M}(\partial_j\hat{M} \times \partial_k\hat{M})$, where $\hat{M} = \mathbf{M}/|\mathbf{M}|$ is the direction of the local magnetization and $\Phi_0 = h/e$ is the flux quantum for a single electron (h is Planck's constant). In the skyrmion lattice, B_{eff} has a topologically quantized average strength of $-\Phi_0$ per area of the magnetic unit cell [for MnSi $B_{\mathrm{eff}} \approx 2.5$ T (*11*)]. B_{eff} induces an effective Lorentz force, which gives rise to an additional "topological" contribution to the Hall effect proportional to the product of B_{eff} and the local polarization of the conduction electrons as observed experimentally (*11*, *17*). Correspondingly, because the electrons are deflected, a force is exerted on the magnetic structure so that there is an efficient "gyromagnetic coupling" (*18*) of the current to the skyrmion lattice (*19*).

From an alternative point of view, the skyrmion lattice may be viewed as an array of circulating dissipationless spin currents, because the skyrmions are characterized by gradients in the spin orienta-

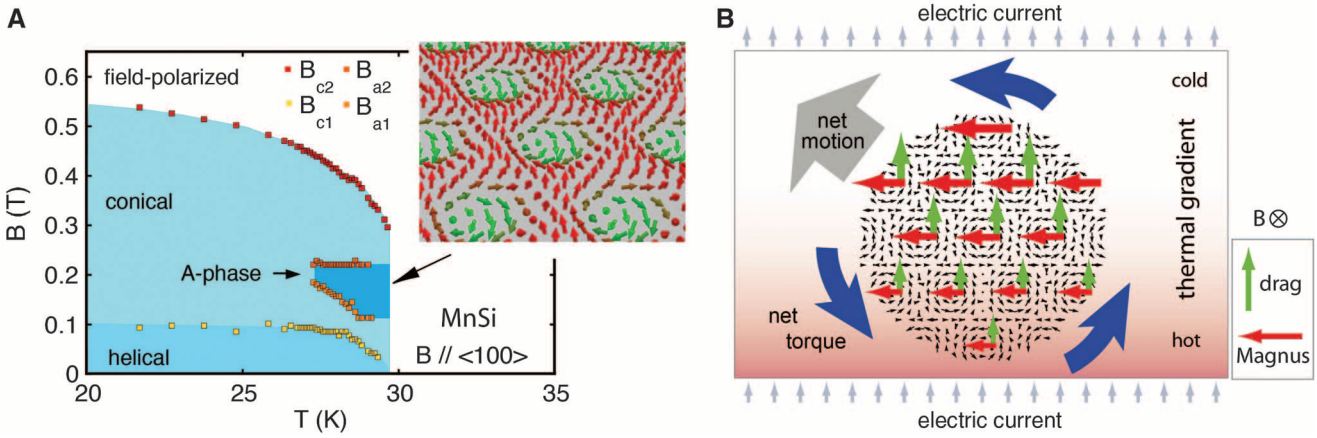

Fig. 1. (**A**) Magnetic phase diagram of MnSi. (Inset) Schematic spin structure of the skyrmion lattice in a plane perpendicular to the applied field. (**B**) Schematic depiction of the spin transfer torque effects on the skyrmion lattice. A temperature gradient induces inhomogeneous Magnus and drag forces and therefore a rotational torque.

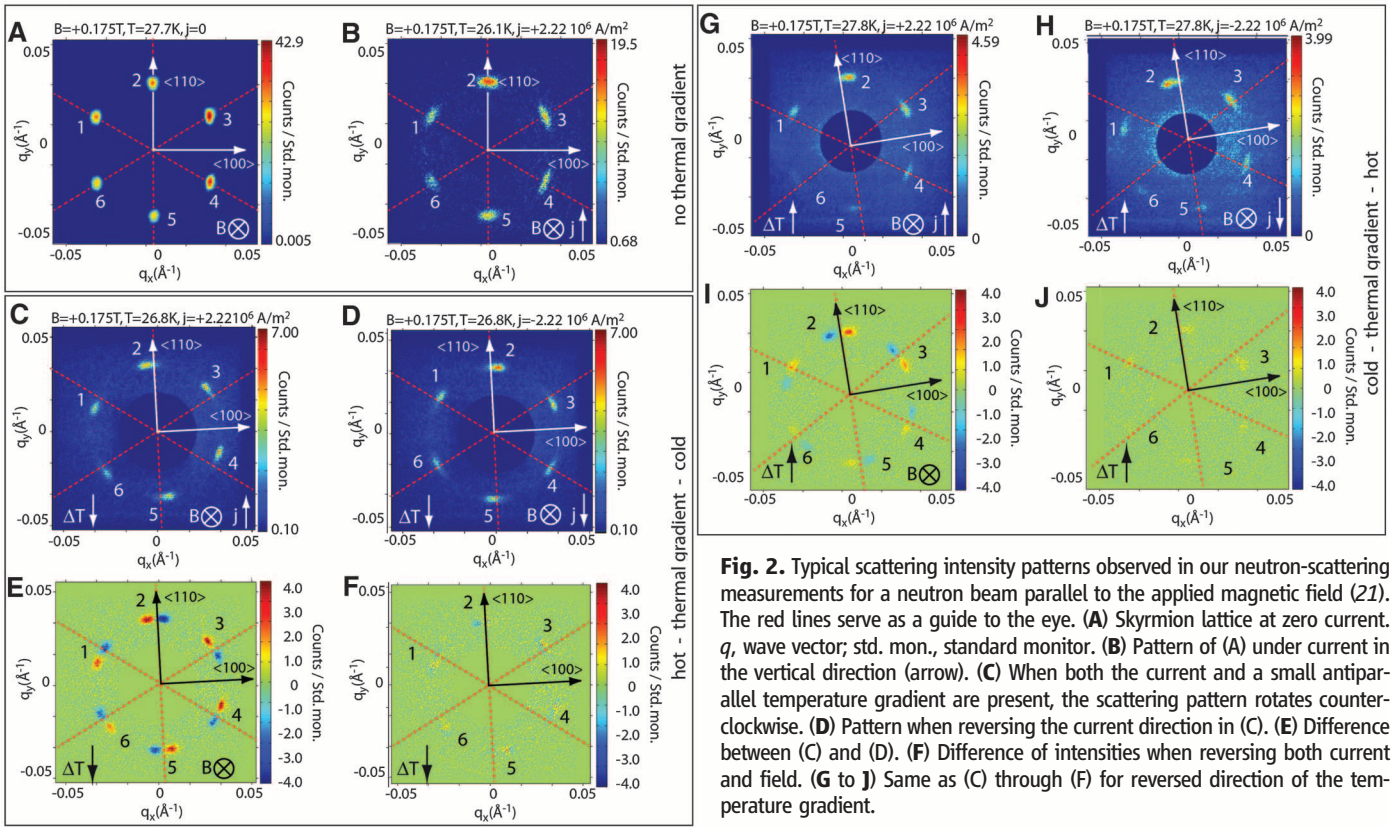

Fig. 2. Typical scattering intensity patterns observed in our neutron-scattering measurements for a neutron beam parallel to the applied magnetic field (*21*). The red lines serve as a guide to the eye. (**A**) Skyrmion lattice at zero current. *q*, wave vector; std. mon., standard monitor. (**B**) Pattern of (A) under current in the vertical direction (arrow). (**C**) When both the current and a small antiparallel temperature gradient are present, the scattering pattern rotates counterclockwise. (**D**) Pattern when reversing the current direction in (C). (**E**) Difference between (C) and (D). (**F**) Difference of intensities when reversing both current and field. (**G** to **J**) Same as (C) through (F) for reversed direction of the temperature gradient.

tion related to their quantized winding number. This is analogous to superconductors, where dissipationless charge currents flow around quantized vortices because of gradients of the phase. When an extra spin current is induced by driving an electric current through the magnetic metal, the spin currents on one side of the skyrmion are enhanced, while they are reduced on the other side. As for a spinning tennis ball, this velocity difference gives rise to a Magnus force acting on the skyrmions. Note, however, that spin (because of spin-orbit coupling) is in contrast to charge not conserved, and therefore this intuitive picture is incomplete. Most importantly, further dissipative forces also arise (*20*), which drag the skyrmions parallel to the current.

In Fig. 1B, this magnetic Magnus force, which is perpendicular to current and field direction, is sketched together with the additional drag forces. The Magnus and drag forces may lead to a translational motion of the skyrmion lattice. However, for the current densities used in our experiment the drift velocity of the electrons and therefore also the drift velocity of the skyrmions is not very large and thus very difficult to detect in a neutron scattering experiment.

In contrast to a translational motion, a rotation is much easier to measure in neutron scattering. Thus, we performed our experiment in the presence of a small temperature gradient parallel to the current, causing the magnetization and therefore the spin currents to vary in magnitude across the domains of the skyrmion lattice. In turn, the strength of the Magnus force varies across the skyrmion lattice (Fig. 1B), inducing a net torque. As estimated below, the torques are sufficiently strong to induce rotations that can be measured directly by neutron scattering.

For our measurements, an electric current was applied along bar-shaped single crystals, where the direction of the current was always perpendicular to the magnetic field and therefore to the skyrmion lines. In Fig. 2, the neutron beam was always collinear to the magnetic field (*21*). The sixfold diffraction pattern of the skyrmion lattice at zero current, $j = 0$ (Fig. 2A), can be compared to the same scattering pattern at a current density, $j = 2.22 \times 10^6$ A m^{-2}, first in a setup minimizing any thermal gradients along the current direction (Fig. 2B). The current was applied along the vertical $[1\bar{1}0]$ direction, whereas the field and the neutron beam were collinear to the line of sight and along [110] (the horizontal direction is along [001]). Under a current, the peaks of the diffraction spots remain in the same location and broaden azimuthally.

We next generated a small temperature gradient along the direction of the current as explained in (*21*). Figure 2C shows the diffraction pattern of the skyrmion lattice for this setup under an electrical current density, $j = 2.22 \times 10^6$ A m^{-2}, which shows a pronounced counterclockwise rotation as compared with Fig. 2, A and B (note that arrows show the technical current direction and the line of sight is opposite to the direction of the neutron beam, consistent with convention). When the current direction is reversed, the rotation changes sign, and the diffraction pattern turns clockwise (Fig. 2D).

There are several unusual aspects of this rotation. First, the entire scattering pattern rotates with respect to its center; that is, all spots move by the same angle even though the electric current has a distinct direction. Second, when reversing either the direction of the current or the direction of the applied field, the sense of the rotation changes sign. This is illustrated in Fig. 2, E and F, which shows the difference of intensity under current reversal and simultaneous reversal of current and field, respectively. For the latter case, the difference of intensities vanishes.

To confirm that the small temperature gradient along the current direction causes the rotation of the scattering pattern, we reversed the direction of the thermal gradient. As illustrated in Fig. 2, G and H, this reverses the sense of rotation with respect to the current and field direction applied in Fig. 2, C and D. Thus the differences of intensity under field reversal, shown in Fig. 2I, are reversed as compared with Fig. 2E (red and blue spots have changed location). When reversing both current and field direction, the difference of the patterns, Fig. 2J, vanishes as before. Lastly, when applying the current along a different crystallographic direction (we tested ⟨111⟩ and an arbitrarily cut sample), the same antisymmetric rotations of the diffraction pattern as a function of magnetic field, electric current, and temperature gradient are observed (*21*).

The detailed rotation as a function of the applied current was determined in systematic measurements for various temperatures and samples. Here, the temperature measured at a specific spot at the surface of the sample (*21*) was kept constant, and temperature gradients had always the same direction. The resulting current dependence of the azimuthal rotation angle ΔΦ, shown for three temperatures as a function of the applied current density in Fig. 3, exhibits a well-defined threshold of order $j_c \approx 10^6$ A m^{-2} above which the rotation begins. For $|j| > j_c$, the entire scattering pattern rotates, and ΔΦ increases steeply with increasing $|j| - j_c$.

Potential parasitic effects cannot explain the observed rotations. First, detailed studies show that there are no changes of orientation of the skyrmion lattice as a function of temperature at $j = 0$ (*10*, *12*, *13*). Second, the temperature difference ΔT between the sample surface and the sample support shows a smooth quadratic increase with current density independent of the direction of the current (Fig. 3B) in contrast to Fig. 3A. Third, for the current densities applied in our study, the Oersted field increases from zero (at the center of the sample) to a value of roughly 1 mT at the surface of the sample, much smaller than the applied magnetic field of 175 mT and therefore negligible. Lastly, for a current parallel to the skyrmion lines or the pristine helimagnetic state, neither a rotation nor a broadening was observed. Interestingly, recent numerical simulations (*22*, *23*) suggest that much larger current densities of the order 10^{12} A m^{-2} may change the orientation of helical magnetic structures.

To explain our experiments, the interplay of three tiny forces has to be considered: (i) spin transfer torques, that is, current induced forces; (ii) pinning forces; and (iii) anisotropy terms. These determine the origin of the rotation, the presence of a threshold, and the angle ΔΦ of the rotated diffraction pattern, respectively. The spin transfer torques can, for example, be described by a Landau-Lifshitz-Gilbert (LLG) equation or variants of Landau-Lifshitz Bloch equations (*24*), which include both reactive and dissipative components representing the Magnus and drag forces mentioned above, respectively. Both are expected to be of the same order of magnitude (*25*). Although the strength of the dissipative forces (related to the parameter β in the LLG equations) is not known, it is possible to estimate the strength of the reactive forces quantitatively.

The size of the Magnus force is given by the product of spin current and the fictitious effec-

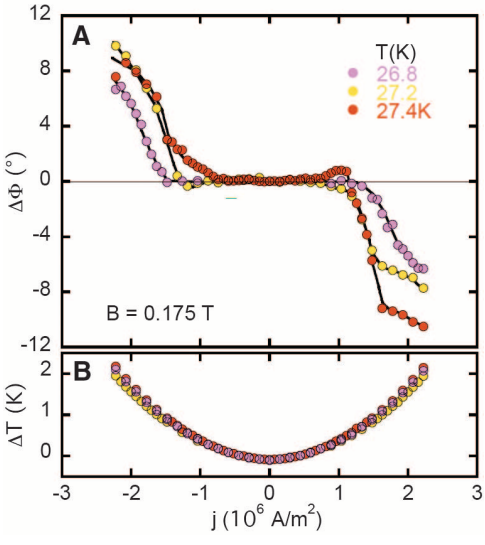

Fig. 3. (**A**) Change of the azimuthal angle of rotation of the scattering pattern as a function of current density for three different temperatures. Data were recorded in a magnetic field of 0.175 T. Above a threshold of 10^6 A m^{-2}, an increasingly strong rotation is observed, where the sign of the rotation depends on the direction of the current. (**B**) Temperature difference between the surface of the sample and the sample holder as a function of current density, where the temperature at the surface of the sample was kept constant for each of the three values given in (A).

tive magnetic field, $f_M \approx ej_s B_{eff}$, and may be estimated as

$$f_M \approx p(T)\frac{j}{10^6\ \mathrm{A\ m^{-2}}}\frac{2.5\times10^6\mathrm{N}}{\mathrm{m}^3}$$
$$\approx p(T)\frac{j}{10^6\ \mathrm{A\ m^{-2}}}\frac{2.7\times10^{-10}k_BT_c}{a^4} \quad (1)$$

where $a \approx 4.58$ Å is the lattice constant of MnSi, k_B is the Boltzmann constant, $T_c \approx 29.5$ K is the ordering temperature, and the local temperature-dependent polarization is defined as the ratio of the spin and charge current densities times the elementary charge, $p(T) = ej_s/j$. For the skyrmion phase, we estimate $p(T) \approx 0.1$ (*11*). The resulting forces at the current densities of 10^6 A m^{-2} studied are much larger than, for example, gravitational forces on the sample, but small when expressed in terms of the microscopic units, k_BT_c/a^4 (compare with Eq. 1), raising the question of why the critical currents j_c are so small.

For $j < j_c$ the current-induced forces are balanced by pinning forces caused by disorder and the underlying regular atomic crystal lattice. The latter may be neglected because of the small spin-orbit interaction (*26*). The discussion presented in (*21*) suggests that even a very strong defect, which locally destroys the magnetization completely, will result in a very small pinning force, less than a few $10^{-5}\ k_BT_c/a$ per impurity, mainly because the magnetization of the skyrmions varies very smoothly. Therefore the observed critical current density j_c together with our estimate, Eq. 1, is consistent with strong pinning defects with a density below 1 part per million. In fact, even though the real density of defects may be higher, their influence may be strongly reduced as the system is in the "collective pinning" regime known, for example, from vortices in superconductors (*27*). Here, pinning forces of random orientation average out to a large extent because of the rigidity of the skyrmion lattice.

The size of the rotation of the skyrmion lattice for $j > j_c$ reflects the balance of the torques τ_M and τ_L due to inhomogeneous Magnus forces and the atomic lattice, respectively. We start by noting, that by symmetry the orientation of a perfect skyrmion lattice (described by a third rank tensor) cannot couple linearly to the current j because of the sixfold rotational symmetry of the lattice. However, a small temperature gradient breaks this symmetry and generates sizable variations of the amplitude of the magnetization and associated polarization $p(T)$ of the electric currents, because the skyrmion phase is only stable close to T_c (compare with Fig. 1). As a result, the Magnus force, Eq. 1, which is proportional to the spin currents and therefore to $p(T)$, will be considerably larger at the "cold" side of the skyrmion lattice than at its "hot" side. This gives rise to a net torque per volume $\tau_M \sim \int \mathbf{r}\times\mathbf{f}_M(\mathbf{r})d^3r/V$. By using Eq. 1 with a spatially varying $p(T)$ and ignoring again dissipative forces for an order of magnitude estimate, we find that the rotational torque per volume, τ_M, in the direction of the fictitious field $\boldsymbol{B}_{eff}$ for a skyrmion lattice domain of size R is given by

$$\tau_M \sim 10^{-10}\frac{\mathbf{j}\cdot\nabla p}{10^6\ \mathrm{A\ m^{-2}}}\frac{R^2}{a}\frac{k_BT_c}{a^3}$$
$$\sim 10^{-5}\frac{k_BT_c}{a^3}\left(\frac{R}{1\ \mathrm{mm}}\right)^2 \quad (2)$$

where we assume $j \approx j_c$ and $\nabla p \approx 0.1/10$ mm.

Note that the effect is proportional to the gradient of the temperature parallel to the current as $\nabla p \approx \frac{\partial p}{\partial T}\nabla T$ (Fig. 1B). Thus τ_M changes sign when either current, magnetic field, or temperature gradient is reversed. The sign of τ_M and all other forces obtained from this analysis (Fig. 1B) is consistent with all our experiments taking into account that charge carriers are holelike as measured experimentally (*11*, *17*). This explains our main experimental results. According to this analysis, the rotational torques arise from temperature-gradient-induced gradients in the spin current. Interestingly, it is more difficult to generate an analogous effect for vortices in superconductors, because charge, as opposed to the spin in skyrmion lattices, is exactly conserved [in (*28*), a rotation of a superconducting vortex lattice has been induced with a bespoke current distribution].

For an estimate of the factor $(R/1\ \mathrm{mm})^2$ in Eq. 2, a lower limit $R > 1$ μm may be inferred from the resolution-limited rocking width of the magnetic Bragg peaks in the skyrmion phase when avoiding demagnetization fields (*21*). Yet, even a small torque τ_M may lead to large rotation angles, because the balancing torque, τ_L, which orients the skyrmion lattice relative to the atomic lattice, is tiny. Only anisotropy terms arising in high power of the spin orbit coupling λ_{SO} contribute to the torque per volume τ_L, which we estimate as (*21*)

$$\tau_L \sim -10^{-2}\lambda_{SO}^4\frac{k_BT_c}{a^3}\sin(6\Phi) \quad (3)$$

For small rotation angles, the torque τ_L grows linearly in the rotation angle Φ. However, in contrast to the torques arising from the inhomogeneous Magnus force, τ_L is independent of the size R of the domains. The rotation angle Φ is finally determined by the balance of τ_M and τ_L. Because of the small prefactor in Eq. 3, $10^{-2}\lambda_{SO}^4$, the large rotation angles observed in our experiments can be explained even for moderately large domains.

It is likely that for $j > j_c$ not only a rotation by an angle sets in but also a linear motion of the magnetic structure, because any rotation of a sizable magnetic domain requires a depinning from defects. For moving domains, spin currents in a frame of reference that is comoving with the domain enter in all formulas given above. Therefore the size of the rotation in the end also depends sensitively on the frictional forces that break Galilean invariance (*25*).

Our observations identify chiral magnets and systems with nontrivial topological properties as ideal systems to advance the general understanding of the effects of spin transfer torques. For instance, spin transfer torques may even be used to manipulate individual skyrmions, recently observed directly in thin samples (*13*). In fact, even complex magnetic structures at surfaces and interfaces may be expected to exhibit the spin torque effects we report here (*29*).

References and Notes

1. J. Slonczewski, *J. Magn. Magn. Mater.* **159**, L1 (1996).
2. L. Berger, *Phys. Rev. B* **54**, 9353 (1996).
3. J. Grollier *et al.*, *Appl. Phys. Lett.* **83**, 509 (2003).
4. M. Tsoi, R. Fontana, S. Parkin, *Appl. Phys. Lett.* **83**, 2617 (2003).
5. M. Tsoi *et al.*, *Phys. Rev. Lett.* **80**, 4281 (1998).
6. E. B. Myers, D. C. Ralph, J. A. Katine, R. N. Louie, R. A. Buhrman, *Science* **285**, 867 (1999).
7. S. I. Kiselev *et al.*, *Nature* **425**, 380 (2003).
8. M. Yamanouchi, D. Chiba, F. Matsukura, H. Ohno, *Nature* **428**, 539 (2004).
9. S. Mühlbauer *et al.*, *Science* **323**, 915 (2009).
10. W. Münzer *et al.*, *Phys. Rev. B* **81**, 041203 (2010).
11. A. Neubauer *et al.*, *Phys. Rev. Lett.* **102**, 186602 (2009).
12. C. Pfleiderer *et al.*, *J. Phys. Condens. Matter* **22**, 164207 (2010).
13. X. Z. Yu *et al.*, *Nature* **465**, 901 (2010).
14. J. Ye *et al.*, *Phys. Rev. Lett.* **83**, 3737 (1999).
15. G. Tatara, H. Kohno, J. Shibata, Y. Lemaho, K.-J. Lee, *J. Phys. Soc. Jpn.* **76**, 054707 (2007).
16. B. Binz, A. Vishwanath, *Physica B* **403**, 1336 (2008).
17. M. Lee, W. Kang, Y. Onose, Y. Tokura, N. P. Ong, *Phys. Rev. Lett.* **102**, 186601 (2009).
18. A. A. Thiele, *Phys. Rev. Lett.* **30**, 230 (1973).
19. C. Pfleiderer, A. Rosch, *Nature* **465**, 880 (2010).
20. S. Zhang, Z. Li, *Phys. Rev. Lett.* **93**, 127204 (2004).
21. Materials and methods are available as supporting material on *Science* Online.
22. O. Wessely, B. Skubic, L. Nordström, *Phys. Rev. Lett.* **96**, 256601 (2006).
23. K. Goto, H. Katsura, N. Nagaosa, Current-induced dynamics of spiral magnet (2008); http://arxiv.org/abs/0807.2901.
24. C. Schieback, D. Hinzke, M. Kläui, U. Nowak, P. Nielaba, *Phys. Rev. B* **80**, 214403 (2009).
25. J. He, Z. Li, S. Zhang, *Phys. Rev. B* **73**, 184408 (2006).
26. D. Belitz, T. R. Kirkpatrick, A. Rosch, *Phys. Rev. B* **73**, 054431 (2006).
27. G. Blatter, M. V. Feigel'man, V. B. Geshkenbein, A. I. Larkin, V. M. Vinokur, *Rev. Mod. Phys.* **66**, 1125 (1994).
28. D. López *et al.*, *Phys. Rev. Lett.* **82**, 1277 (1999).
29. M. Bode *et al.*, *Nature* **447**, 190 (2007).

30. We thank B. Binz, S. Dunsiger, E. M. Forgan, C. Franz, E. Hering, M. Janoschek, H. Kolb, M. Laver, S. Legl, T. Lorenz, A. H. MacDonald, T. Nattermann, J. Peters, S. M. Ramos da Silva, B. Russ, T. Schulz, R. Schwikowski, B. Spivak, A. Vishwanath, M. Vojta, M. Wagner, W. Zwerger, and the team of FRM II for discussions and support. We gratefully acknowledge financial support through SFB608 and TRR80, SFB/TR12 of the German Science Foundation (Deutsche Forschungsgemeinschaft), the Deutsche Telekom Stiftung (K.E.), NSF grant PHY05-51164 (A.R.), and by Stichting voor Fundamenteel Onderzoek der Materie, Nederlandse Organisatie voor Wetenschappelijk Onderzoek, and the European Research Council (R.A.D.).

Supporting Online Material

www.sciencemag.org/cgi/content/full/330/6011/1648/DC1
Materials and Methods
SOM Text
Figs. S1 to S8
Table S1
References

27 July 2010; accepted 18 November 2010
10.1126/science.1195709